ACS APPLIED MATERIALS & INTERFACES

Research Article

www.acsami.org

Insight into the Capacitive Properties of Reduced Graphene Oxide

Wei Zhang,[†,§] Yuxia Zhang,[†,§] Yang Tian,[‡] Zhiyu Yang,[†] Qingqing Xiao,[†] Xin Guo,[†] Lin Jing,[†] Yufei Zhao,[†] Yiming Yan,*[,†] Jinsheng Feng,*[,†] and Kening Sun*[,†]

[†]School of Chemical Engineering and Environment, Beijing Institute of Technology, Beijing 100081, China

[‡]College of Life and Environmental Science, Minzu University of China, Beijing 100081, China

ABSTRACT: Graphene-based materials have been widely used as electrode materials of supercapacitors. However, the intrinsic properties related to the capacitance of graphene-based materials essentially need to be clarified. In this work, we have prepared reduced graphene oxide (RGO) through a simple chemical reduction strategy by using hydrazine hydrate as the reducing reagent. The different reduction levels of graphene sheets were successfully realized by controlling the chemical reduction time, and the surface state and density of the functional group were precisely adjusted. We investigated the electrochemical performance of the as-prepared RGO electrode materials. A time dependence of the specific capacitance for the as-prepared RGO electrode was observed. Graphene oxide reduced by hydrazine hydrate at 95 °C for 60 min exhibited the highest weight specific capacitance. The RGO samples were systematically characterized with Fourier transform infrared (FTIR) spectra, X-ray photoelectron spectroscopy (XPS), and Raman measurements. We conclude that the oxygen-containing groups, electrical conductivity, density of defects, and carbon electronic state play substantial roles in deciding the specific capacitance of reduced graphene oxide.

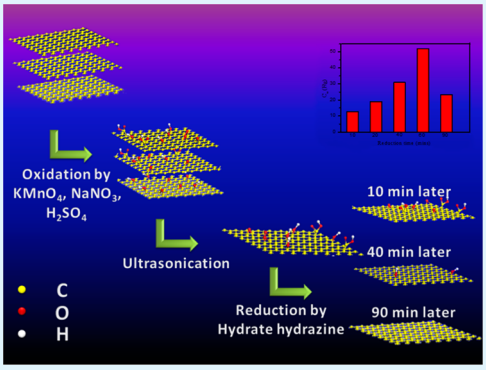

KEYWORDS: *graphene oxide, capacitance, chemical reduction, hydrazine hydrate*

INTRODUCTION

Graphene-based materials have attracted extensive research attention as excellent electrode materials due to their theoretical properties and practical advantages, such as high surface area, large electrical conductivity, unique heterogeneous electron transfer, and charge carrier rates.[1−3] In particular, they have found numerous applications in electrochemical fields, such as energy storage and generation.[4−6] The most outstanding feature of graphene materials is the theoretically high specific surface area up to 2675 $m^2 \cdot g^{-1}$. As such, one can calculate the intrinsic capacitance of the graphene nanosheet to be 21 $\mu F \cdot cm^{-2}$ and a weight-specific capacitance of 550 $F \cdot g^{-1}$, assuming that the entire 2675 $m^2 \cdot g^{-1}$ is fully utilized. This value sets the upper limit of electric double-layer (EDL) capacitance for carbon-based materials.

In the past years, many efforts have been devoted to developing a graphene-based supercapacitor. However, most of these documented works mainly focus on the incorporation of metal oxides or polymers with graphene material, resulting in functionalized nanocomposites, to introduce pseudo-capacitance for supercapacitor applications.[7−10] Noteworthy, according to the reported results, we found that the weight-specific capacitance of the graphene-based supercapacitors showed very different values varying from 6.57 to 128 $F \cdot g^{-1}$.[11−16] Unfortunately, all these reported values are only 1.2−21.8% of the theoretical capacitance of graphene materials. Therefore, it is interesting to raise a crucial question: what are the key factors affecting the capacitance of graphene-based materials? As far as we are aware, this subject has been largely overlooked by the researchers in the past several years.

Recently, Lee et al. reported the tunable electrochemical activity of graphene materials by a controllable electrochemical reducing process.[17] They showed that the electrochemical properties of graphene materials could be controlled by mandatory tailoring of the surface functional group of graphene, suggesting a relationship between surface state and the electrochemical properties of graphene materials. In addition, Kötz et al. revealed that the capacitance of graphene materials may associate with their layer instance.[18] They showed the dependence of capacitance on structural properties of graphene. More recently, Pumera et al. discussed the effect of preparation methods on the electrochemistry of graphene materials, where they demonstrated that the capacitance of graphene materials was also strongly dependent on the preparation methods.[19,20] All in all, these works throw light on a fundamental understanding of the intrinsic capacitance of graphene materials. Unfortunately, these studies did not provide enough understanding of the capacitive properties of graphene-base material. For example, the effect of the preparation process itself on the capacitance of graphene materials has been largely neglected. We anticipate that such a study not only complements the previous work to get further

Received: May 23, 2013
Accepted: January 23, 2014
Published: January 23, 2014

   dx.doi.org/10.1021/am4057562 | *ACS Appl. Mater. Interfaces* 2014, 6, 2248−2254

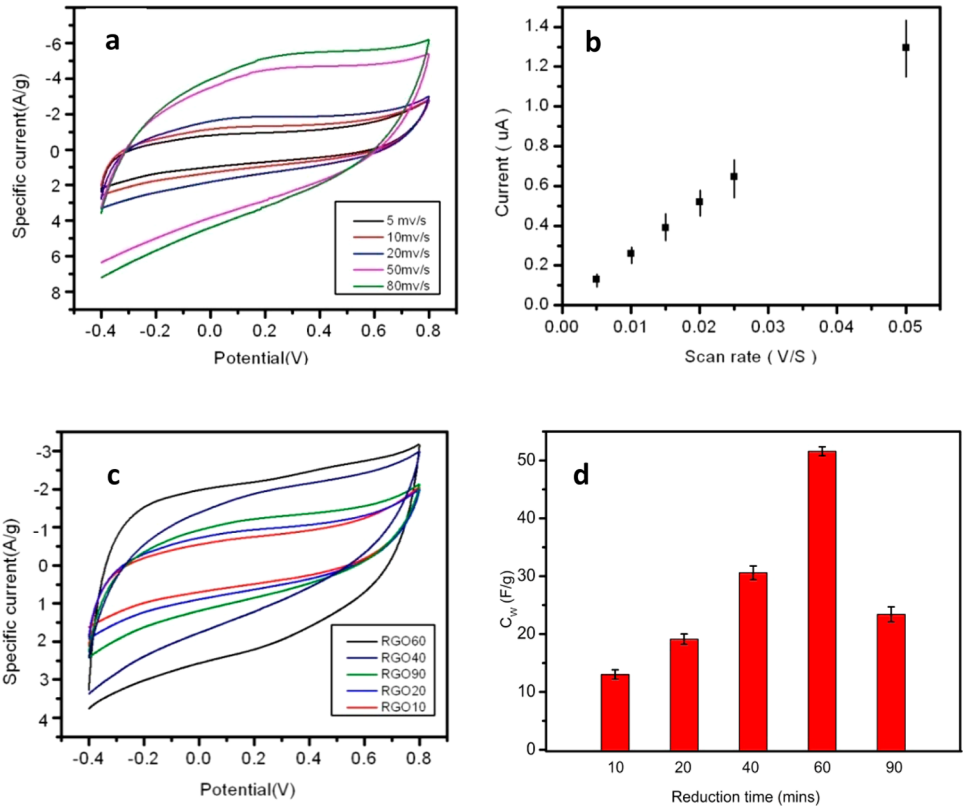

Figure 1. (a) CVs of the as-prepared RGO60-modified ITO electrode at different scan rate from 5 to 80 mV·s^{-1} in 2.0 M H_2SO_4. (b) A plot of the charge current obtained from CVs with the scan rate for RGO60. (c) CVs of different RGO samples at a scan rate of 15 mV·s^{-1} in 2.0 M H_2SO_4. (d) Weight-specific capacitances of GO, RGO10, RGO20, RGO40, RGO60, and RGO90.

insight into the capacitance mechanism but also provides useful information for rational design and synthesis of graphene-based materials by optimizing the synthetic parameters for high-performance energy storage devices.

In this work, we prepared the chemically reduced graphene oxide by using hydrazine hydrate as the reducing reagent. Different reduced levels of GO were easily realized in a facile and controllable manner. The effect of the reduction time on the capacitance of reduced graphene oxide was carefully examined. By using different characterization methods, such as cyclic voltammograms (CVs), Fourier transform infrared (FTIR) spectra, X-ray photoelectron spectroscopy (XPS), and Raman, we demonstrate that the oxygen-containing groups, electric conductivity, density of defects, and carbon electric state present clearly a synergic effect on the capacitance of reduced graphene oxide (RGO). We showed that, in our case, RGO with 60 min reduction at 95 °C by hydrazine hydrate possesses the highest specific capacitance.

RESULTS AND DISCUSSION

Graphene-based materials generally include the graphene oxide, reduced graphene oxide, and graphene. Graphene is usually obtained by reducing the graphene oxide with different methods. In this context, we prepared the reduced graphene oxide with a chemical reduction method. First, graphene oxide was synthesized from graphite according to a modified Hummer's method.[21] Then, the reduced graphene oxide (RGO) was prepared by chemically reducing graphene oxide for different reduction times with hydrazine hydrate. The acronyms of RGO10, RGO20, RGO40, RGO60, and RGO90 were used to refer to the corresponding samples which were obtained at different reduction times of 10, 20, 40, 60, and 90 min, respectively.

The capacitance of the samples was examined in a three-electrode system in which a Pt slide was used as counter electrode and saturated calomel electrode (SCE) was used as reference electrode. CVs were performed to evaluate the capacitance. Generally, the baseline current of the CVs represents the capacitive charge−discharge current, and the weight-specific capacitance of the examined samples can be calculated with the equation

$$C_w = I/(\nu M) \quad (1)$$

where C_w is the weight-specific capacitance (F/g); I is the current; M is the mass of coated RGO sample on the ITO electrode; and ν is the scan rate of the CV experiment.

To exclude the electrochemical reaction caused by the active species in solution, the solution was thoroughly deoxygenated before the test, and the CVs were then measured in a potential window from −0.4 to 0.8 V at different scan rates. Figure 1a shows the CV curves of RGO60 at various scan rates in 2.0 M H_2SO_4 electrolyte. As seen, the CV curves at different scan rate exhibit a similar box-like shape with a nearly rectangular shape at the potential range, indicating good charge propagation within the tested sample. Noteworthy, we did not observe apparent pseudo-capacitance from the CVs for the chemical reduction derived RGO60 sample. This is in good agreement with the observation which has been previously reported by Vivekchand et al.[22] This could be explained by the fact that less electroactive groups were produced at the surface of RGO by using the chemical reduction method than that produced through a thermal reduction route. The capacitive currents

dx.doi.org/10.1021/am4057562 | ACS Appl. Mater. Interfaces 2014, 6, 2248−2254

were measured upon several potential values (n = 6) and were plotted as a function of various scan rates (Figure 1b). As a result, the C_w of RGO60 was calculated to be 51.85 F·g^{-1}. Figure 1c compares the CV curves measured with all the as-prepared RGO samples in 2.0 M H_2SO_4 electrolyte at a scan rate of 15 mV·s^{-1}. We normalized the current with the mass of the modified samples and found a clear dependence of the capacitive current of the as-prepared samples on reduction time. Figure 1d displays the graphical comparison of the C_w calculated with all RGO samples. The weight-specific capacitances are 12.63, 18.94, 30.88, 51.85, and 23.26 F·g^{-1} for RGO10, RGO20, RGO40, RGO60, and RGO90, respectively. It can be seen that the capacitance increased significantly with the increase of the reduction time until the time reaches to 60 min. Subsequently, the capacitance decreased dramatically upon a longer reduction time of 90 min. We repeated the experiments and obtained the same tendency to verify the interesting phenomena.

We first examined FTIR spectra of the samples to investigate how the functional group located at the reduced graphene oxide changes along with the reduction time to explain the above observed results. Figure 2a compares the typical FTIR spectra

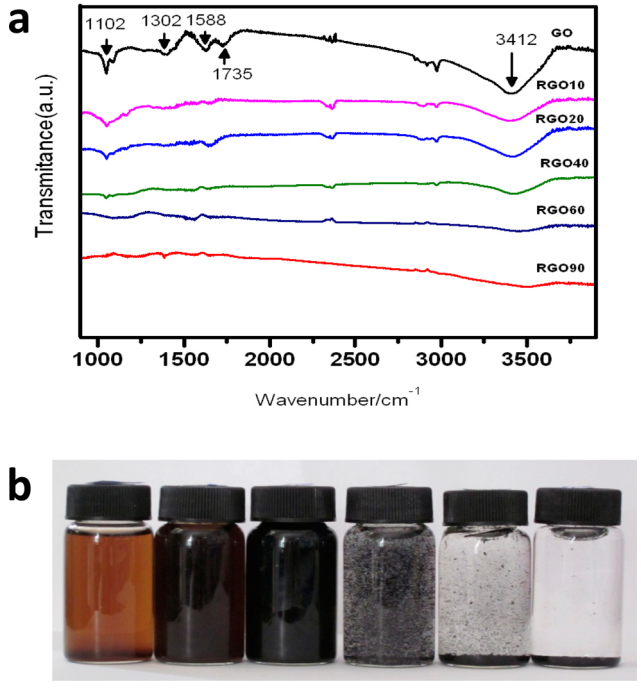

Figure 2. (a) FTIR spectra of the GO and as-prepared RGO samples. (b) Optical pictures of the aqueous dispersion of GO and RGO samples (1.0 g·L^{-1}). From left to right: GO, RGO10, RGO20, RGO40, RGO60, and RGO90.

of GO and RGO samples. The characteristic features of GO can be identified as a broad and intense peak at 3412 cm^{-1} (O−H stretching vibrations) and the peaks at 1735 cm^{-1} (C═O stretching vibrations from carbonyl and carboxylic groups), 1588 cm^{-1} (Cis═C skeletal vibrations from unoxidized graphitic domains), and 1102 cm^{-1} (C−O stretching vibrations). In addition, a relatively weak stretching vibration peak of C−OH at 1302 cm^{-1} also was observed. In comparison, the intensity of all peaks of RGO samples was decreased with the increase of the reduction time. Particularly, the peaks corresponding to −OH, C−O, and C═O stretching vibrations were almost indistinguishable after 40 min reduction, suggesting that most oxygen-containing functional groups were effectively removed in a reduction process. It was noted that, for RGO90, all peaks corresponding to oxygen-containing functional groups nearly disappeared, indicating that the GO has been sufficiently reduced by hydrazine hydrate.

It is well known that the existence of an oxygen-containing group on the surface of carbon materials (CNTs, graphene etc.) exhibits good hydrophilic ability. Therefore, it is reasonable to anticipate that the removal of oxygen-containing functional groups from the surface of GO may enhance the hydrophobic ability. To verify this, Figure 2b gives the optical images of the samples dispersed in aqueous solution. Even after 60 min static staying, a yellow and homogeneous suspension of GO in water was observed. It suggests that the GO has strong hydrophilic ability due to the presence of large amounts of functional groups (hydroxyl and epoxy functional groups in the basal plane and carbonyl and carboxyl groups at the sheet edges) which were produced during the preparing procedure. As a comparison, the color of RGO samples turns black gradually with the increase of reduction time. The RGO40 shows many aggregations after 60 min static staying, while the RGO90 exhibits much more poor insoluble property with black precipitations. The phenomenon strongly demonstrates that the functional group of oxygen containing could be successively suppressed with the increase of reduction time. As a consequence, the removal of the oxygen-containing group leads to enhanced hydrophobic ability, thus resulting in aggregation of RGO samples due to hydrophobic interaction of the RGO sheets in aqueous solution. Thus, it is assumed to decrease the surface area of the samples, therefore decreasing the capacitance. To verify this, we conducted the Brunauer−Emmett−Teller (BET) measurements to determine the surface area of the RGO samples. The results showed that the surface areas were 136, 130, 123, 120, and 115 m^2·g^{-1}, for RGO10, RGO20, RGO40, RGO60, and RGO90, respectively. We then normalized the capacitance with the surface area, and the corresponding values were 92, 145.7, 251.1, 432.1, and 202.2 μF·m^{-2}. A tendency similar to that shown in Figure 1d was observed, indicating that the observed change of RGO capacitive performances should arise from the chemical surface features rather than the structural properties.

Meanwhile, the electrical conductivity is an important parameter regarding the capacitance of carbon materials. To probe the effect of the functional groups on the electrical conductivity, we measured the electrical conductivity of the prepared samples with a dc four-probe method using the Source Meter 2400. As shown in Table 1, similar to the results reported elsewhere,[23] the GO reveals very low electrical conductivity of 4.19 × 10^{-8} S cm^{-1}, which may be either contributed from carboxyl, carbonyl, hydroxyl, and epoxy

Table 1. Electrical Conductivity of the GO and RGO Samples

	GO	RGO10	RGO20	RGO40	RGO60	RGO90
electrical conductivity (S·cm^{-1})	4.19 × 10^{-8}	1.14 × 10^{-4}	8.25 × 10^{-2}	0.14	1.13	3.45

dx.doi.org/10.1021/am4057562 | ACS Appl. Mater. Interfaces 2014, 6, 2248−2254

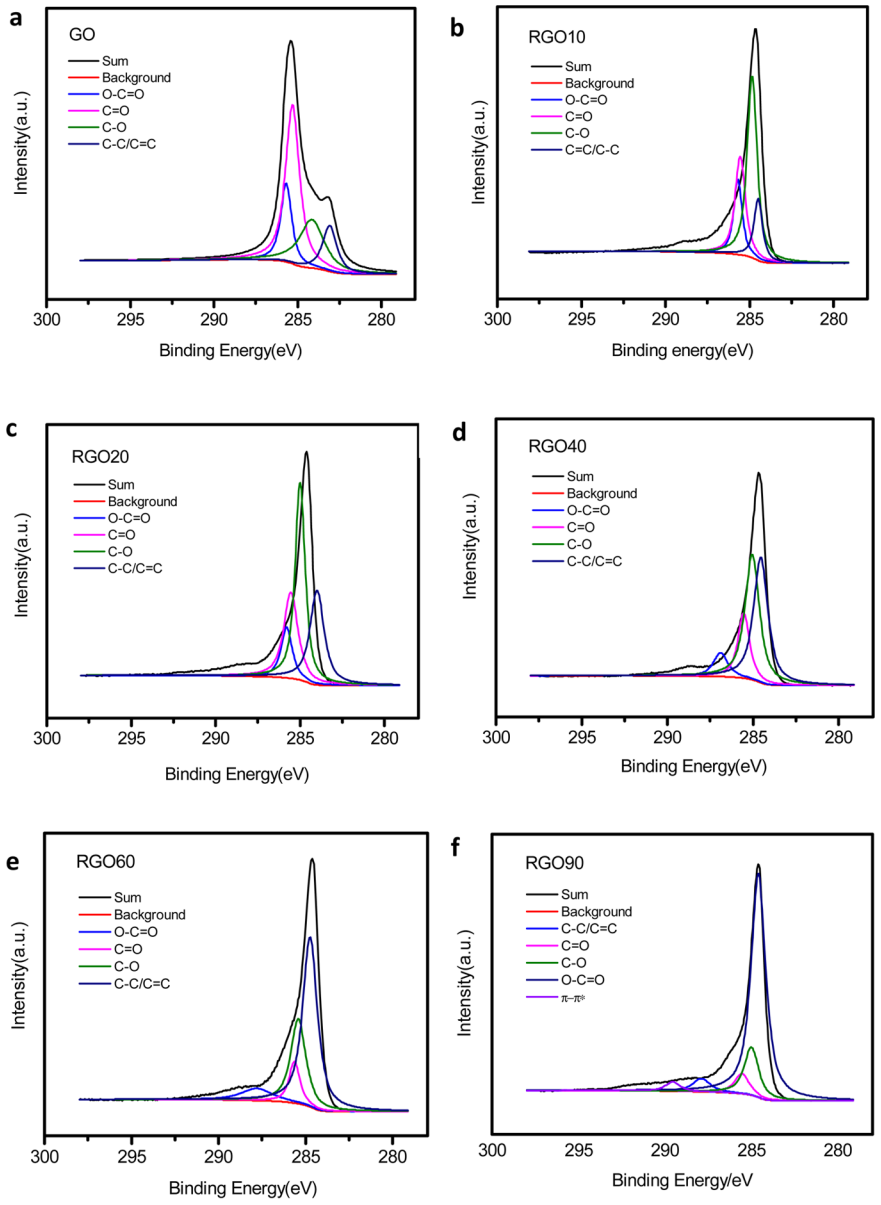

Figure 3. C(1s) XPS spectra obtained with (a) GO, (b) RGO10, (c) RGO20, (d) RGO40, (e) RGO60, and (f) RGO90.

groups or due to other atomic-scale lattice defects of GO.[24] Meanwhile, the electrical conductivity of the reduced samples was found to increase from 1.14×10^{-4} to 3.45 S cm^{-1} along with the reduction time from 10 to 90 min. The improved electrical conductivity of RGO samples should be attributed to the removal of oxygen-containing groups or caused by the possible restoration of the aromatic and conjugated system in graphene.

To clearly understand the effect of reduction time on the capacitance, we make a preliminary analysis upon the obtained results. It is known that the overall capacitance of carbon-based materials consists of pseudo-capacitance and double-layer capacitance. The former is based on faradic, redox reactions which arise from the electrochemical active groups on the surface, and the latter comes from the charge accumulated at the electrode/electrolyte interface. In our case, on one hand, an increase of reduction time may lead to the removal of the oxygen-containing group, resulting in a loss of pseudo-capacitance; on the other hand, the removal of the oxygen-containing group contributes to an increase of the electrical conductivity and thus improves the electrical double-layer capacitance. However, as shown in Figure 1c, we did not observe significant faradic current from the CVs of the RGO samples, suggesting that the pseudo-capacitance of the samples is not a predominant part of the overall capacitance of the RGO. Consequently, we deduce that the successive removal of the oxygen-containing group along with the reduction time should not be used to fully explain the change of the capacitance of the RGO samples.

Thus, to gain further insight into the capacitive property of the RGO samples, we attempted to employ XPS to analyze the functional groups and electronic state of elements on the surface of GO and RGO and exploit their detailed effects on the capacitive properties. Figure 3 shows the C (1s) XPS spectra of the GO and RGO samples, which consist of four main components arising from C−O (hydroxyl and epoxy, ∼284.4 eV), C═O (carbonyl, ∼285.6 eV), C═C/C−C (∼283.9 eV), and O−C═O (carboxyl, ∼286.5 eV) groups.[25] At the

dx.doi.org/10.1021/am4057562 | ACS Appl. Mater. Interfaces 2014, 6, 2248−2254

beginning of the reduction, we found that the carbonyl groups were first transformed into C−O bonds. This can be clearly evident by comparing the RGO10 sample with the GO sample, from which a quick decrease of the peak at ∼285.6 eV and a corresponding increase of the peak of ∼284.4 eV were observed. Subsequently, the carbonyl groups were continuously removed along with the increase of reduction time, as seen from Figure 3c−f. Meanwhile, the peak of ∼284.4 eV displays an apparent increase as shown in Figure 3b,c and then a decrease (Figure 3d−f). It implies an interesting change of the C−O groups on the surface along with the increase of reduction time. As a comparison, the peak of O−C═O exhibits a remarkable decrease in RGO20 and RGO30 samples, suggesting that its reduction needs more time compared with carbonyl groups. Interestingly, the peak at ∼283.9 eV shows a slow increase (Figure 3a−d) and then a quick increase (Figure 3e,f). As a consequence, it seems that the C═C/C−C at the surface is prone to be produced at the later stage of the process. Therefore, we believe that the aromatic carbon ring structure is much easier to recover after a long time reaction in hydrazine hydrate. This assumption is strongly supported by the appearance of a significant $\pi-\pi^*$ shake-up satellite peak at around 290.8 eV for RGO90, indicating the enhanced aromatic or conjugated state in the structure of RGO90.[26] It should be noted that some oxygen-containing groups are still maintained even in the sample of RGO90, which is consistent with FTIR results.

Raman spectroscopy is a powerful tool to characterize the ordered/disordered crystal structures of carbonaceous materials.[27] We finally utilized Raman to further examine the structural changes of RGO samples. The typical characteristics of carbon materials in Raman spectra are the G band (1580 cm^{-1}), which is generally assigned to the E_{2g} phonon of sp^2 bonds of carbon atoms, and the D band (1350 cm^{-1}) as a breathing mode of k-point phonons of A_{1g} symmetry, which is ascribed to local defects and disorders, particularly the defects located at the edges. Figure 4 shows the Raman spectra of GO and RGO samples. The intensity ratios of the D to G bands (I_D/I_G) were calculated and listed in Table 2. It can be seen that the I_D/I_G of all RGO samples are apparently larger than that of GO. As the reduction time was increased, the I_D/I_G value of RGO samples was found to increase gradually. In other words, it indicates the increase of disorder degree of carbon atoms and the decrease in size of sp^2 clusters in the RGO samples.

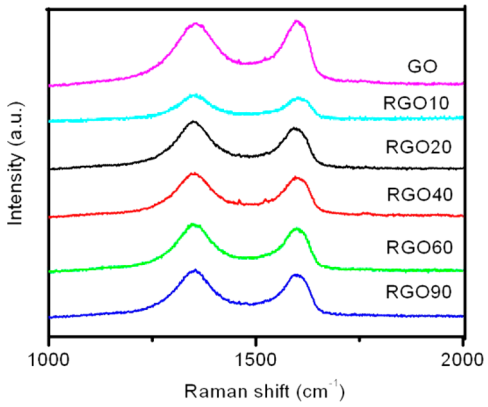

Figure 4. Raman spectra obtained with GO and different RGO samples.

Table 2. Comparisons of the I_D/I_G Values Calculated from the Raman Spectrum of the GO and RGO Samples

	GO	RGO10	RGO20	RGO40	RGO60	RGO90
I_D/I_G	0.93	1.124	1.192	1.247	1.296	1.031

However, we found that the I_D/I_G value of RGO90 is smaller than that of RGO60. It is known that the smaller I_D/I_G peak intensity ratio of a Raman spectrum indicates lower defects of the graphitized structures containing the disorders caused at the edges.[28] Therefore, the small I_D/I_G value of RGO90 could be reasonably ascribed to the appearance of the $\pi-\pi^*$ shake-up satellite peak at RGO90, as shown in the XPS results. It is generally accepted that the defective carbon atoms at the edge sites have stronger electron charge and transport ability than that of the carbon rings. For the RGO90 sample, we deduced that the recovery of aromatic carbon rings, as shown in XPS, and the decrease of I_D/I_G, as shown in Raman, may be directly related to the observed decrease of specific capacitance.

Finally, we tried to make a comprehensive analysis to clarify the key factors affecting the capacitance of RGO. As shown above, we have demonstrated a clear removal process of oxygen-containing groups from the surface of RGO along with chemical reduction by hydrazine hydrate. Consequently, it improves the electrical conductivity of the RGO samples, leading to fast charge propagation of the RGO samples and an increase of electric double-layer interfacial capacitance. In our case, the electric double-layer interfacial capacitance of the chemical reduced GO is predominant, as shown in CVs. Thereby, the improved electrical conductivity can explain why there is a continuous increase of specific capacitance of RGO with the increase of reduction time at the first stage. However, the XPS and Raman further indicated that the density of defects on the surface of RGO was not constant during the reduction process. We found that a recovery of the aromatic carbon ring occurred along with the prolonged chemical reduction in hydrazine hydrate solution, resulting in a substantial decrease of capacitance of the RGO samples.[20] Therefore, it is reasonable to draw a conclusion that a synergic effect contributed from the electric conductivity and the defect density should decide the observed specific capacitance of the RGO samples.

CONCLUSIONS

In this paper, we have investigated the effect of chemical reduction time on the specific capacitance of RGO. We observed a time-dependent specific capacitance of the as-prepared RGO samples. A series of characterizations including CVs, FTIR, hydrophobic ability, XPS, and Raman were conducted. We found that an oxygen-containing group from the RGO sample was successively removed along with the chemical reduction. As a consequence, it, on one hand, leads to an increase of electrical conductivity which is contributed to improve the specific capacitance of the RGO samples and, on the other hand, leads to a recovery of aromatic carbon rings and decreases the density of defects which imparts the specific capacitance of the RGO samples. Due to such a synergic effect, the RGO60 sample shows the highest weight-specific capacitance of 51.85 $F{\cdot}g^{-1}$. Although the specific capacitance of the RGO obtained here is not significantly superior to that of other reported results, our work provides a symmetric understanding of capacitive properties of RGO. The findings may offer useful information for optimizing and tailoring the

structure of graphene-based materials for their applications as high performance supercapacitors.

METHODS AND MEASURMENTS

Synthesis. Flake graphite was purchased from Alfa Aesar. Sulfuric acid (98%), hydrogen peroxide (30%), hydrochloric acid (5%), sodium nitrate, and potassium permanganate were purchased from the Beijing Chemical Works. Hydrazine hydrate (85%) was purchased from the Tianjin Bodi Chemical Holding Co., Ltd. All reagents used were of analytical grade. Deionized water (>18.4 MΩ cm^{-1}) was produced with a Milli-Q machine.

Graphite oxide was synthesized referring to the modified Hummers's method.[21] Typically, graphite powder (2.0 g) and concentrated H_2SO_4 (86.0 mL) were added into a round flask in an ice bath with magnetic stirring for ten minutes. Then, sodium nitrate (2.0 g) and potassium permanganate (16.0 g) were added slowly into the solution while keeping the reaction temperature at 0 °C. After 30 min, the mixture was kept at 35 °C for 1.0 h. Then, deionized water (180 mL) was added into the system at 95 °C and reacted for 1.0 h. After that, hydrogen peroxide (12 mL) was added into the mixture with magnetic stirring at 95 °C for 2 h. The final product was washed and centrifuged repeatedly with 5% HCL to remove sulfate ions and finally washed with deionized water until the pH of the filtrate solution was 7.0. The obtained slurry of graphite oxide was then dried at 50 °C for 36 h in an air-dry oven. Graphene oxide was obtained by ultrasonicating a 0.5 mg/mL suspension of graphite oxide in deionized water for 4 h.

Reduced graphene oxide (RGO) was synthesized by reducing graphene oxide with hydrazine hydrate under different reaction times. The suspension of graphene oxide (30 mL, 0.5 mg/mL) and hydrazine hydrate (15.5 μl) was mixed into a round flask with magnetic stirring at 95 °C. The mass ratio of graphene oxide and hydrazine hydrate was 10:8. After a reaction time of 10, 20, 40, 60, and 90 min, the obtained samples were RGO10, RGO20, RGO40, RGO60, and RGO90, respectively. The final products were washed and centrifuged repeatedly with deionized water to remove the residual hydrazine hydrate. Finally, the product was dried at 50 °C for 36 h in an oven under Ar atmosphere.

Characterizations. The characterizations of the as-prepared RGO samples were conducted with FTIR, Raman, and XPS. Fourier transform infrared (FTIR) spectra were recorded with a Bio-Rad FTIR spectrometer FTS 165. Raman spectra were obtained on an RM 2000 microscopic confocal Raman spectrometer (Renishaw in via Plus, England) employing a 514 nm laser beam. X-ray photoelectron spectroscope (XPS) spectra were recorded on a PHI Quantear SXM (ULVAC-PH INC) in which Al was used as an anode probe in 6.7×10^{-8} Pa. X-ray diffraction (XRD, X′ Pert PRO MPD) spectra were recorded with an area detector operating under a voltage of 40 kV and a current of 40 mA using Cu Kα radiation (λ = 0.15418 nm).

Electrochemical Measurements. Electrochemical measurements were carried out on a CHI660C electrochemical workstation (Chenhua Instrument, China). Before the measurement, 1.0 mg of RGO was dispersed in 0.5 mL of DMF and ultrasonicated strongly for 30 min resulting in a suspension with a concentration of 2.0 mg/mL. Then, the suspension was dropped onto a cleaned ITO (1 cm × 3 cm) electrode. In the conventional three-electrode system, the RGO-modified ITO electrode was used as a working electrode. The Pt wire and saturated calomel electrode (SCE) served as the counter electrode and reference electrode, respectively. The electrolyte was 2.0 M H_2SO_4. CV curves were recorded at a potential range from −0.4 to 0.8 V at different scanning rates.

AUTHOR INFORMATION

Corresponding Authors

*Fax: +86-10-68918696. E-mail: yanym@bit.edu.cn.
*E-mail: analchemie@bit.edu.cn.
*E-mail: bitkeningsun@163.com.

Author Contributions

[§]These authors contributed equally to this work.

Notes

The authors declare no competing financial interest.

ACKNOWLEDGMENTS

Financial support from Ministry of Science and Technology (2012DFR40240), National Natural Science Foundation of China (Grant Nos. 21175012), and Chinese Ministry of Education (Project of New Century Excellent Talents in University) is gratefully acknowledged.

REFERENCES

(1) Wang, Y.; Shi, Z. Q.; Huang, Y.; Ma, Y. F.; Wang, C. Y.; Chen, M. M.; Chen, Y. S. Supercapacitor devices based on graphene materials. *J. Phys. Chem. C* **2009**, *113*, 13103−13107.

(2) Stoller, M. D.; Park, S. J.; Zhu, Y. W.; An, J. H.; Ruoff, R. S. Graphene-based ultracapacitors. *Nano Lett.* **2008**, *8*, 3498−3502.

(3) Sun, Z. Z.; James, D. K.; Tour, J. M. Graphene chemistry: Synthesis and manipulation. *J. Phys. Chem. Lett.* **2011**, *2*, 2425−2432.

(4) Wang, G. X.; Yang, J.; Park, J.; Gou, X. L.; Wang, B.; Liu, H.; Yao, J. Facile synthesis and characterization of graphene nanosheets. *J. Phys. Chem. C* **2008**, *112*, 8192−8195.

(5) Simon, P.; Gogotsi, Y. Materials for electrochemical capacitors. *Nature Mater.* **2008**, *7*, 845−854.

(6) Wang, D. H.; Choi, D.; Li, J.; Yang, Z. G.; Nie, Z. M.; Kou, R.; Hu, D. H.; Wang, C. M.; Saraf, L. V.; Zhang, J. G.; Aksay, L. A.; Liu, J. Self-assembled TiO_2−graphene hybrid nanostructures for enhanced Li-ion insertion. *ACS Nano* **2009**, *3*, 907−914.

(7) Xue, Y. H.; Liu, Y.; Lu, F.; Qu, J.; Chen, H.; Dai, L. M. Functionalization of graphene oxide with polyhedral oligomeric silsesquioxane (POSS) for multifunctional applications. *J. Phys. Chem. Lett.* **2012**, *3*, 1607−1612.

(8) Xu, J. J.; Wang, K.; Zu, S. Z.; Han, B. H.; Wei, Z. X. Hierarchical nanocomposites of polyaniline nanowire arrays on graphene oxide sheets with synergistic effect for energy storage. *ACS Nano* **2010**, *4*, 5019−5026.

(9) Wang, D. W.; Li, F.; Zhao, J. P.; Ren, W. C.; Chen, Z. G.; Tan, J.; Wu, Z. S.; Gentle, L.; Lu, G. Q.; Cheng, H. M. Fabrication of graphene/polyaniline composite paper via in situ anodic electropolymerization for high-performance flexible electrode. *ACS Nano* **2009**, *3*, 1745−1752.

(10) Wang, B.; Wang, Y.; Park, J.; Ahn, H.; Wang, G. X. In situ synthesis of Co_3O_4/graphene nanocomposite material for lithium-ion batteries and supercapacitors with high capacity and supercapacitance. *J. Alloys Compd.* **2011**, *509*, 7778−7783.

(11) Peng, X. Y.; Liu, X. X.; Diamond, D.; Lau, K.T. Synthesis of electrochemically-reduced graphene oxide film with controllable size and thickness and its use in supercapacitor. *Carbon* **2011**, *49*, 3488−3496.

(12) Jeong, H. K.; Jin, M. H.; Ra, E. J.; Sheem, K. Y.; Han, G. H.; Arepalli, S.; Lee, Y. H. Enhanced electric double layer capacitance of graphite oxide intercalated by poly(sodium 4-styrensulfonate) with high cycle stability. *ACS Nano* **2010**, *4*, 1162−1166.

(13) Biswas, S.; Drzal, L. T. Multilayered nano-architecture of variable sized graphene nanosheets for enhanced supercapacitor electrode performance. *ACS Appl. Mater. Interfaces* **2010**, *2*, 2293−2300.

(14) Wang, H. W.; Hu, Z. A.; Chang, Y. Q.; Chen, Y. L.; Zhang, Z. Y.; Yang, Y. Y.; Wu, H. Y. Preparation of reduced graphene oxide/cobalt oxide composites and their enhanced capacitive behaviors by homogeneous incorporation of reduced graphene oxide sheets in cobalt oxide matrix. *Mater. Chem. Phys.* **2011**, *130*, 672−679.

(15) Chen, Y.; Zhang, X.; Yu, P.; Ma, Y. W. Electrophoretic deposition of graphene nanosheets on nickel foams for electrochemical capacitors. *J. Power Sources* **2010**, *195*, 3031−3035.

(16) Le, L. T.; Ervin, M. H.; Qiu, H. W.; Fuchs, B. E.; Lee, W. Y. Graphene supercapacitor electrodes fabricated by inkjet printing and thermal reduction of graphene oxide. *Electrochem. Commun.* **2011**, *13*, 355−358.
(17) Uhm, S.; Tuyen, N. H.; Lee, J. Controlling oxygen functional species of graphene oxide for an electro-oxidation of l-ascorbic acid. *Electrochem. Commun.* **2011**, *13*, 677−680.
(18) Hantel, M. M.; Kaspar, T.; Nesper, R.; Wokaun, A.; Kötz, R. Partially reduced graphite oxide for supercapacitor electrodes: Effect of graphene layer spacing and huge specific capacitance. *Electrochem. Commun.* **2011**, *13*, 90−92.
(19) Buglione, L.; Chng, E. L. K.; Ambrosi, A.; Sofer, Z.; Pumera, M. Graphene materials preparation methods have dramatic influence upon their capacitance. *Electrochem. Commun.* **2012**, *14*, 5−8.
(20) Ambrosi, A.; Bonanni, A.; Sofer, Z.; Cross, J. S.; Pumera, M. Electrochemistry at chemically modified graphenes. *Chem.—Eur. J.* **2011**, *17*, 10763−10770.
(21) Hummers, W. S.; Offeman, R. E. Preparation of graphitic oxide. *J. Am. Chem. Soc.* **1958**, *80*, 1339−1339.
(22) Vivekchand, S. R. C.; Rout, C. S.; Subrahmanyam, K. S.; Govindaraj, A.; Rao, C. N. R. Graphene-based electrochemical supercapacitors. *J. Chem. Sci.* **2008**, *120*, 9−13.
(23) Zhang, K.; Zhang, L. L.; Zhao, X. S.; Wu, J. Graphene/polyaniline nanofiber composites as supercapacitor electrodes. *Chem. Mater.* **2010**, *22*, 1392−1401.
(24) Rutter, G. M.; Crain, J. N.; Guisinger, N. P.; Li, T.; First, P. N.; Stroscio, J. A. Scattering and interference in epitaxial graphene. *Science* **2007**, *317*, 219−222.
(25) Szabó, T.; Berkesi, O.; Forgó, P.; Josepovits, K.; Sanakis, Y.; Petridis, D.; Dekany, I. Evolution of surface functional groups in a series of progressively oxidized graphite oxides. *Chem. Mater.* **2006**, *18*, 2740−2749.
(26) Fan, X.; Peng, W.; Li, Y.; Li, X.; Wang, S.; Zhang, G.; Zhang, F. Deoxygenation of exfoliated graphite oxide under alkaline conditions: A green route to graphene preparation. *Adv. Mater.* **2008**, *20*, 4490−4493.
(27) Dresselhaus, M. S.; Jorio, A.; Hofmann, M.; Dresselhaus, G.; Saito, R. Perspectives on carbon nanotubes and graphene raman spectroscopy. *Nano Lett.* **2010**, *10*, 751−758.
(28) Zhou, Y.; Bao, Q. L.; Tang, L. A. L.; Zhong, Y. L.; Loh, K. P. Hydrothermal dehydration for the "green" reduction of exfoliated graphene oxide to graphene and demonstration of tunable optical limiting properties. *Chem. Mater.* **2009**, *21*, 2950−2956.